

Multi-dimensional constraint relativistic mean field model and applications in actinide and transfermium nuclei

Bing-Nan Lu¹, Jie Zhao¹, En-Guang Zhao^{1,2} and Shan-Gui Zhou^{1,2*}

¹State Key Laboratory of Theoretical Physics, Institute of Theoretical Physics, Chinese Academy of Sciences, Beijing 100190, China

²Center of Theoretical Nuclear Physics, National Laboratory of Heavy Ion Accelerator, Lanzhou 730000, China

PACS REF: 21.60.Jz, 24.75.+i, 25.85.-w, 27.90.+b

Nov 14, 2013

Abstract

In this contribution we present some results of potential energy surfaces of actinide and transfermium nuclei from multi-dimensional constrained relativistic mean field (MDC-RMF) models. Recently we developed multi-dimensional constrained covariant density functional theories (MDC-CDFT) in which all shape degrees of freedom $\beta_{\lambda\mu}$ with even μ are allowed and the functional can be one of the following four forms: the meson exchange or point-coupling nucleon interactions combined with the non-linear or density-dependent couplings. In MDC-RMF models, the pairing correlations are treated with the BCS method. With MDC-RMF models, the potential energy surfaces of even-even actinide nuclei were investigated and the effect of triaxiality on the fission barriers in these nuclei was discussed. The non-axial reflection-asymmetric β_{32} shape in some transfermium nuclei with $N = 150$, namely ^{246}Cm , ^{248}Cf , ^{250}Fm , and ^{252}No were also studied.

1. Introduction

The occurrence of spontaneous symmetry breaking in atomic nuclei leads to various nuclear shapes which can usually be described by the parametrization of the nuclear surface or the nucleon density distribution [1, 2]. In mean-field calculations, the following parametrization

$$\beta_{\lambda\mu} = \frac{4\pi}{3AR^\lambda} \langle Q_{\lambda\mu} \rangle, \quad (1)$$

is usually used, where $Q_{\lambda\mu}$ are the mass multipole operators. In Fig. 1, a schematic show is given for some typical nuclear shapes. The majority of observed nuclear shapes is of spheroidal form which is usually described by β_{20} . Higher-order deformations with $\lambda > 2$ such as β_{30} also appear in certain atomic mass regions [3]. In addition, non-axial shapes in atomic nuclei, in particular, the nonaxial-quadrupole (triaxial) deformation β_{22} has been studied both experimentally and theoretically [4–6]. The influence of the nonaxial octupole β_{32} deformation on the low-lying spectra has been also investigated [7–16].

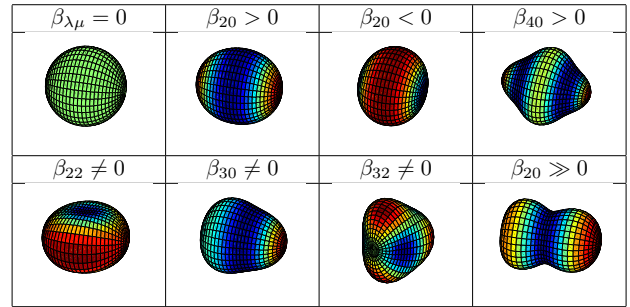


Fig. 1: (Color online) A schematic show of some typical nuclear shapes. From left to right, the 1st row: (a) Sphere, (b) Prolate spheroid, (c) Oblate spheroid, (d) Hexadecapole shape, and the second row: (e) Triaxial ellipsoid, (f) Reflection symmetric octupole shape, (g) Tetrahedron, (h) Reflection asymmetric octupole shape with very large quadrupole deformation and large hexadecapole deformation. Taken from Ref. [17].

In nuclear fission study, various shape degrees of freedom play important and different roles in the occurrence and in determining the heights of the inner and outer barriers in actinide nuclei (in these nuclei double-humped fission barriers usually appear). For example, the inner fission barrier is usually lowered when the triaxial deformation is allowed, while for the outer barrier the reflection asymmetric (RA) shape is favored [18–22, 24, 25].

In order to give a microscopic and self-consistent description of the potential energy surface (PES) with more shape degrees of freedom included, multi-dimensional constrained covariant density functional theories were developed recently [26, 27]. In these theories, all shape degrees of freedom $\beta_{\lambda\mu}$ with even μ are allowed. In this contribution, we present two recent applications of these theories: the PES's of actinide nuclei and the non-axial reflection-asymmetric β_{32} shape in some transfermium nuclei. In Section 2, the formalism of our multi-dimensional constrained covariant density functional theories will be given

*e-mail: sgzhou@itp.ac.cn

briefly. The results and discussions are presented in Section 3. Finally we give a summary in Section 4.

2. Formalism

The details of the formalism for covariant density functional theories can be found in Refs. [28–33]. The CDFT functional in our multi-dimensional constrained calculations can be one of the following four forms: the meson exchange or point-coupling nucleon interactions combined with the non-linear or density-dependent couplings [26, 27, 34, 35]. Here we show briefly the one corresponding to the non-linear point coupling (NL-PC) interactions. The starting point of the relativistic NL-PC density functional is the following Lagrangian:

$$\mathcal{L} = \bar{\psi}(i\gamma_\mu\partial^\mu - M)\psi - \mathcal{L}_{\text{lin}} - \mathcal{L}_{\text{nl}} - \mathcal{L}_{\text{der}} - \mathcal{L}_{\text{Cou}}, \quad (2)$$

where

$$\begin{aligned} \mathcal{L}_{\text{lin}} &= \frac{1}{2}\alpha_S\rho_S^2 + \frac{1}{2}\alpha_V\rho_V^2 + \frac{1}{2}\alpha_{TS}\vec{\rho}_{TS}^2 + \frac{1}{2}\alpha_{TV}\vec{\rho}_{TV}^2, \\ \mathcal{L}_{\text{nl}} &= \frac{1}{3}\beta_S\rho_S^3 + \frac{1}{4}\gamma_S\rho_S^4 + \frac{1}{4}\gamma_V[\rho_V^2]^2, \\ \mathcal{L}_{\text{der}} &= \frac{1}{2}\delta_S[\partial_\nu\rho_S]^2 + \frac{1}{2}\delta_V[\partial_\nu\rho_V]^2 + \frac{1}{2}\delta_{TS}[\partial_\nu\vec{\rho}_{TS}]^2 \\ &\quad + \frac{1}{2}\delta_{TV}[\partial_\nu\vec{\rho}_{TV}]^2, \\ \mathcal{L}_{\text{Cou}} &= \frac{1}{4}F^{\mu\nu}F_{\mu\nu} + e\frac{1-\tau_3}{2}A_0\rho_V, \end{aligned} \quad (3)$$

are the linear coupling, nonlinear coupling, derivative coupling, and the Coulomb part, respectively. M is the nucleon mass, α_S , α_V , α_{TS} , α_{TV} , β_S , γ_S , γ_V , δ_S , δ_V , δ_{TS} , and δ_{TV} are coupling constants for different channels and e is the electric charge. ρ_S , $\vec{\rho}_{TS}$, ρ_V , and $\vec{\rho}_{TV}$ are the isoscalar density, isovector density, time-like components of isoscalar current, and time-like components of isovector current, respectively. The densities and currents are defined as

$$\begin{aligned} \rho_S &= \bar{\psi}\psi, & \vec{\rho}_{TS} &= \bar{\psi}\vec{\tau}\psi, \\ \rho_V &= \bar{\psi}\gamma^0\psi, & \vec{\rho}_{TV} &= \bar{\psi}\vec{\tau}\gamma^0\psi. \end{aligned} \quad (4)$$

Starting from the above Lagrangian, using the Slater determinants as trial wave functions and neglecting the Fock term as well as the contributions to the densities and currents from the negative energy levels, one can derive the equations of motion for the nucleons,

$$\hat{h}\psi_i = (\boldsymbol{\alpha} \cdot \vec{p} + \beta(M + S(\vec{r})) + V(\vec{r}))\psi_i = \epsilon_i\psi_i, \quad (5)$$

where the potentials $V(\mathbf{r})$ and $S(\mathbf{r})$ are calculated as

$$\begin{aligned} S &= \alpha_S\rho_S + \beta_S\rho_S^2 + \gamma_S\rho_S^3 + \delta_S\Delta\rho_S \\ &\quad + (\alpha_{TS}\rho_{TS} + \delta_{TS}\Delta\rho_{TS})\tau_3, \end{aligned} \quad (6)$$

$$\begin{aligned} V &= \alpha_V\rho_V + \gamma_V\rho_V^3 + \delta_V\Delta\rho_V \\ &\quad + (\alpha_{TV}\rho_{TV} + \delta_{TV}\Delta\rho_{TV})\tau_3. \end{aligned} \quad (7)$$

An axially deformed harmonic oscillator (ADHO) basis is adopted for solving the Dirac equation [26, 27, 36]. The ADHO basis is defined as the eigen solutions of the Schrodinger equation with an ADHO potential [37, 38],

$$\left[-\frac{\hbar^2}{2M}\nabla^2 + V_B(z, \rho)\right]\Phi_\alpha(\mathbf{r}\sigma) = E_\alpha\Phi_\alpha(\mathbf{r}\sigma), \quad (8)$$

where

$$V_B(z, \rho) = \frac{1}{2}M(\omega_\rho^2\rho^2 + \omega_z^2z^2), \quad (9)$$

is the axially deformed HO potential and ω_z and ω_ρ are the oscillator frequencies along and perpendicular to z axis, respectively. These basis states are also eigen functions of the z component of the angular momentum j_z with eigen values $K = m_l + m_s$. For any basis state $\Phi_\alpha(\mathbf{r}\sigma)$, the time reversal state is defined as $\Phi_{\bar{\alpha}}(\mathbf{r}\sigma) = \mathcal{T}\Phi_\alpha(\mathbf{r}\sigma)$, where $\mathcal{T} = i\sigma_y K$ is the time reversal operator and K is the complex conjugation. Apparently we have $K_{\bar{\alpha}} = -K_\alpha$ and $\pi_{\bar{\alpha}} = \pi_\alpha$. These basis states form a complete set for expanding any two-component spinors. For a Dirac spinor with four components,

$$\psi_i(\mathbf{r}\sigma) = \begin{pmatrix} \sum_\alpha f_i^\alpha \Phi_\alpha(\mathbf{r}\sigma) \\ \sum_\alpha g_i^\alpha \Phi_\alpha(\mathbf{r}\sigma) \end{pmatrix}, \quad (10)$$

where the sum runs over all the possible combination of the quantum numbers $\alpha = \{n_z, n_r, m_l, m_s\}$, and f_i^α and g_i^α are the expansion coefficients. In practical calculations, one should truncate the basis in a proper way [26, 27, 36].

The nucleus is assumed to be symmetric under the V_4 group, that is, all the potentials and densities can be expanded as

$$f(\rho, \varphi, z) = f_0(\rho, z)\frac{1}{\sqrt{2\pi}} + \sum_{n=1}^{\infty} f_n(\rho, z)\frac{1}{\sqrt{\pi}}\cos(2n\varphi), \quad (11)$$

The PES is obtained by the constrained self-consistent calculation,

$$E' = E_{\text{RMF}} + \sum_{\lambda\mu} \frac{1}{2}C_{\lambda\mu}Q_{\lambda\mu}, \quad (12)$$

where the variables $C_{\lambda\mu}$'s change their values during the iteration.

Both the BCS approach and the Bogoliubov transformation are implemented in our model to take into account the pairing effects. For convenience, we name the MDC-CDFT with the BCS approach for the pairing as the MDC-RMF model and that with the Bogoliubov transformation as the MDC-RHB model. More details of the multi-dimensional constraint covariant density functional theories can be found in Refs. [26, 27].

3. Results and discussions

3.1. PES's of actinides

In Refs. [26, 27], one- (1-d), two- (2-d), and three-dimensional (3-d) constrained calculations were performed

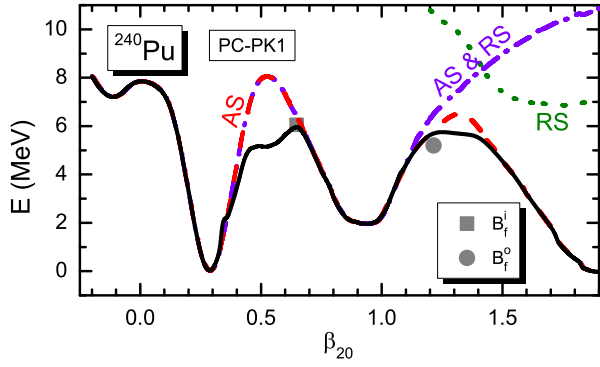


Fig. 2: (Color online) Potential energy curves of ^{240}Pu with various self-consistent symmetries imposed. The solid black curve represents the calculated fission path with V_4 symmetry imposed: the red dashed curve is that with axial symmetry (AS) imposed, the green dotted curve that with reflection symmetry (RS) imposed, the violet dot-dashed line that with both symmetries (AS & RS) imposed. The empirical inner (outer) barrier height B_{emp} is denoted by the grey square (circle). The energy is normalized with respect to the binding energy of the ground state. The parameter set used is PC-PK1. Taken from Ref. [26].

for the actinide nucleus ^{240}Pu . The MDC-RMF model with the parameter set PC-PK1 [39] was used. In Fig. 2 we show the 1-d potential energy curves from an oblate shape with β_{20} about -0.2 to the fission configuration with β_{20} beyond 2.0 which are obtained from calculations with different self-consistent symmetries imposed: the axial (AS) or triaxial (TS) symmetries combined with reflection symmetric (RS) or asymmetric cases. The importance of the triaxial deformation on the inner barrier and that of the octupole deformation on the outer barrier are clearly seen: The triaxial deformation reduces the inner barrier height by more than 2 MeV and results in a better agreement with the empirical value [22]; the RA shape is favored beyond the fission isomer and lowers very much the outer fission barrier [21]. Besides these features, it was found for the first time that the outer barrier is also considerably lowered by about 1 MeV when the triaxial deformation is allowed. In addition, a better reproduction of the empirical barrier height can be seen for the outer barrier. It has been stressed that this feature can only be found when the axial and reflection symmetries are simultaneously broken [26].

Two-dimensional PES's in the (β_{20}, β_{22}) plane near the inner and outer barriers are shown in Figs. 3 and 4, respectively. Starting from the axially symmetric ground state, the nucleus goes through the triaxial valley to the isometric state. The inner barrier is located at $\beta_{20} \approx 0.65$ and $\beta_{22} \approx 0.06$. The isomeric state keeps an axially symmetric shape. As β_{20} further increases, the nucleus goes through a triaxial valley again, and then goes fission. The outer barrier is located at $\beta_{20} \approx 1.21$, $\beta_{22} \approx 0.02$, and $\beta_{30} \approx 0.37$.

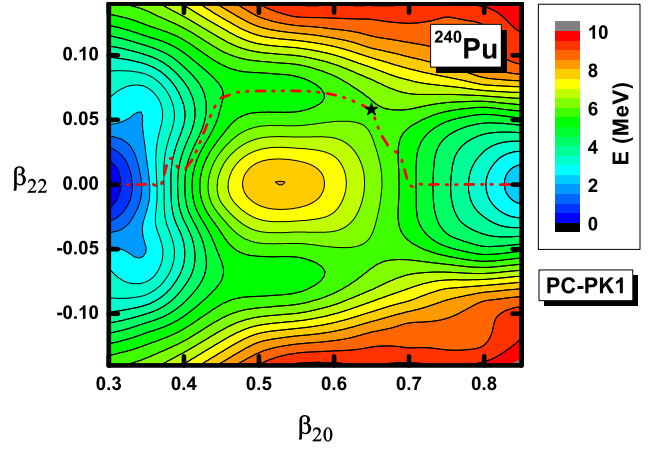


Fig. 3: (Color online) Potential energy surfaces of ^{240}Pu in the (β_{20}, β_{22}) plane around the inner barrier. The energy is normalized with respect to the binding energy of the ground state. The least-energy fission path is represented by a dash-dotted line. The saddle point is denoted by the full star. The contour interval is 0.5 MeV.

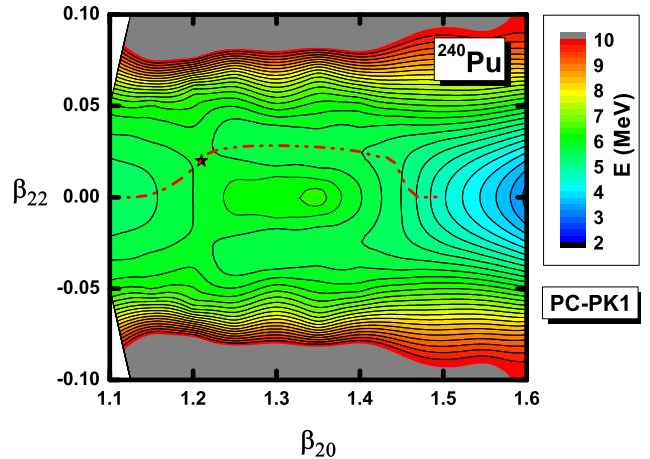


Fig. 4: (Color online) Potential energy surfaces of ^{240}Pu in the (β_{20}, β_{22}) plane around the outer barrier. The energy is normalized with respect to the binding energy of the ground state. The least-energy fission path is represented by a dash-dotted line. The saddle point is denoted by the full star. The contour interval is 0.25 MeV.

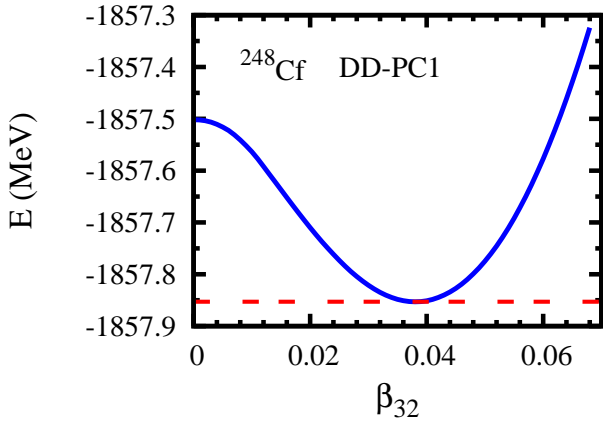


Fig. 5: (Color online) The binding energy E (relative to the ground state) for ^{248}Cf as a function of the non-axial octupole deformation parameter β_{32} .

A systematic study of even-even actinide nuclei has been carried out and the results were presented in Ref. [27] where we have shown that the triaxial deformation lowers the outer barriers of these actinide nuclei by about $0.5 \sim 1$ MeV (about $10 \sim 20\%$ of the barrier height).

3.2. Y_{32} -correlations in $N = 150$ isotones

It has been anticipated that the tetrahedral shape ($\beta_{\lambda\mu} = 0$, if $\lambda \neq 3$ and $\mu \neq 2$) may appear in the ground states of some nuclei with special combinations of the neutron and proton numbers [9, 12, 16]. The tetrahedral symmetry-driven quantum effects may also lead to a large increase of binding energy in superheavy nuclei [40]. However, no solid experimental evidence has been found for nuclei with tetrahedral shapes. On the other hand, β_{32} deformation may appear together with other shape degrees of freedom, say, β_2 . For example, it has been proposed that the non-axial octupole Y_{32} -correlation results in the experimentally observed low-energy 2^- bands in the $N = 150$ isotones [41] and the RASM calculations reproduces well the experimental observables of these 2^- bands [42].

In Ref. [43] the non-axial reflection-asymmetric β_{32} deformation in $N = 150$ isotones, namely ^{246}Cm , ^{248}Cf , ^{250}Fm , and ^{252}No was investigated using the MDC-RMF model with the parameter set DD-PC1 [44]. It was found that due to the interaction between a pair of neutron orbitals, $[734]9/2$ originating from $\nu j_{15/2}$ and $[622]5/2$ originating from $\nu g_{9/2}$, and that of a pair of proton orbitals, $[521]3/2$ originating from $\pi f_{7/2}$ and $[633]7/2$ originating from $\pi i_{13/2}$, rather strong non-axial octupole Y_{32} effects appear in ^{248}Cf and ^{250}Fm which are both well deformed with large axial-quadrupole deformations, $\beta_{20} \approx 0.3$.

In Fig. 5, the potential energy curve, i.e., the total binding energy as a function of β_{32} was shown for ^{248}Cf . At each point of the potential energy curve, the energy is minimized automatically with respect to other shape degrees of freedom such as β_{20} , β_{22} , β_{30} , and β_{40} , etc. One finds

in this curve a clear pocket with the depth more than 0.3 MeV. Similar potential energy curve was also obtained for ^{250}Fm . For ^{246}Cm and ^{252}No , only a shallow minimum develops along the β_{32} shape degree of freedom. It was also shown that the evolution of the non-axial octupole β_{32} effect along the $N = 150$ isotonic chain is not very sensitive to the form of the energy density functional and the parameter set we used [43].

Both the non-axial octupole parameter β_{32} and the energy gain due to the β_{32} -distortion reach maximal values at ^{248}Cf in the four nuclei along the $N = 150$ isotonic chain [43]. This is consistent with the analysis given in Refs. [42, 45] and the experimental observation that in ^{248}Cf , the 2^- state is the lowest among these nuclei [41]. These results indicate a strong Y_{32} -correlation in these nuclei.

4. Summary

In this contribution we present the formalism and some applications of the multi-dimensional constrained relativistic mean field (MDC-RMF) models in which all shape degrees of freedom $\beta_{\lambda\mu}$ with even μ are allowed. The potential energy surfaces (curves) of actinide nuclei and the effect of the triaxiality on the first and second fission barriers were investigated. It is found that besides the octupole deformation, the triaxiality also plays an important role upon the second fission barriers. The non-axial reflection-asymmetric β_{32} shape in $N = 150$ isotones were studied and rather strong non-axial octupole Y_{32} effects have been found in ^{248}Cf and ^{250}Fm which are both well deformed with large axial-quadrupole deformations, $\beta_{20} \approx 0.3$.

Acknowledgement

This work has been supported by Major State Basic Research Development Program of China (Grant No. 2013CB834400), National Natural Science Foundation of China (Grant Nos. 11121403, 11175252, 11120101005, 11211120152, and 11275248), the Knowledge Innovation Project of Chinese Academy of Sciences (Grant No. KJCX2-EW-N01). The results described in this paper are obtained on the ScGrid of Supercomputing Center, Computer Network Information Center of Chinese Academy of Sciences.

References

- [1] Bohr A and Mottelson B R 1998 *Nuclear Structure* vol I (World Scientific)
- [2] Ring P and Schuck P 1980 *The Nuclear Many-Body Problem* (Springer-Verlag Berlin, Heidelberg, and New York)
- [3] Butler P A and Nazarewicz W 1996 *Rev. Mod. Phys.* **68** 349–421

- [4] Starosta K, et al. 2001 *Phys. Rev. Lett.* **86** 971–974
- [5] Odegard S W, et al. 2001 *Phys. Rev. Lett.* **86** 5866–5869
- [6] Meng J and Zhang S Q 2010 *J. Phys. G: Nucl. Phys.* **37** 064025–12
- [7] Hamamoto I, Mottelson B, Xie H and Zhang X Z 1991 *Z. Phys. D* **21** 163–175
- [8] Skalski J 1991 *Phys. Rev. C* **43** 140–145
- [9] Li X and Dudek J 1994 *Phys. Rev. C* **49** R1250–R1252
- [10] Takami S, Yabana K and Matsuo M 1998 *Phys. Lett. B* **431** 242–248
- [11] Yamagami M, Matsuyanagi K and Matsuo M 2001 *Nucl. Phys. A* **693** 579–602
- [12] Dudek J, Gozdz A, Schunck N and Miskiewicz M 2002 *Phys. Rev. Lett.* **88** 252502–4
- [13] Dudek J, Curien D, Dubray N, Dobaczewski J, Pangon V, Olbratowski P and Schunck N 2006 *Phys. Rev. Lett.* **97** 072501–4
- [14] Olbratowski P, Dobaczewski J, Powalowski P, Sadziak M and Zborecki K 2006 *Int. J. Mod. Phys. E* **15** 333–338
- [15] Zborecki K, Magierski P, Heenen P H and Schunck N 2006 *Phys. Rev. C* **74** 051302(R)–5
- [16] Dudek J, Gozdz A, Mazurek K and Moliq H 2010 *J. Phys. G: Nucl. Phys.* **37** 064032–16
- [17] Lu B N 2012 *Multi-dimensional constrained relativistic mean field theory and the potential energy surfaces and fission barriers of actinide nuclei* Ph.D. thesis Institute of Theoretical Physics, Chinese Academy of Sciences in Chinese
- [18] Pashkevich V V 1969 *Nucl. Phys. A* **133** 400–404
- [19] Möller P and Nilsson S G 1970 *Phys. Lett. B* **31** 283–286
- [20] Girod M and Grammaticos B 1983 *Phys. Rev. C* **27** 2317–2339
- [21] Rutz K, Maruhn J A, Reinhard P G and Greiner W 1995 *Nucl. Phys. A* **590** 680–702
- [22] Abusara H, Afanasjev A V and Ring P 2010 *Phys. Rev. C* **82** 044303–11
- [23] Abusara H, Afanasjev A V and Ring P 2012 *Phys. Rev. C* **85** 024314–17
- [24] Prassa V, Nikšić T, Lalazissis G A and Vretenar D 2012 *Phys. Rev. C* **86** 024317–12
- [25] Prassa V, Nikšić T and Vretenar D 2013 *Phys. Rev. C* **88** 044324–11
- [26] Lu B N, Zhao E G and Zhou S G 2012 *Phys. Rev. C* **85** 011301(R)–5 (*Preprint* 1110.6769)
- [27] Lu B N, Zhao J, Zhao E G and Zhou S G 2013 arXiv:1304.2513 [nucl-th]
- [28] Serot B D and Walecka J D 1986 *Adv. Nucl. Phys.* **16** 1–327
- [29] Reinhard P G 1989 *Rep. Prog. Phys.* **52** 439–514
- [30] Ring P 1996 *Prog. Part. Nucl. Phys.* **37** 193–263
- [31] Vretenar D, Afanasjev A, Lalazissis G and Ring P 2005 *Phys. Rep.* **409** 101–259
- [32] Meng J, Toki H, Zhou S G, Zhang S Q, Long W H and Geng L S 2006 *Prog. Part. Nucl. Phys.* **57** 470–563 (*Preprint* nucl-th/0508020)
- [33] Nikšić T, Vretenar D and Ring P 2011 *Prog. Part. Nucl. Phys.* **66** 519–548
- [34] Lu B N, Zhao J, Zhao E G and Zhou S G 2012 *EPJ Web Conf.* **38** 05003 (*Preprint* 1303.0621)
- [35] Lu B N, Zhao J, Zhao E G and Zhou S G 2013 arXiv:1304.6830 [nucl-th] Proceedings of the XXXVI Mexican Symposium on Nuclear Physics, Cocoyoc, Morelos, Mexico, Jan. 7-10, 2013
- [36] Lu B N, Zhao E G and Zhou S G 2011 *Phys. Rev. C* **84** 014328–10 (*Preprint* 1104.4638)
- [37] Gambhir Y K, Ring P and Thimet A 1990 *Ann. Phys.* **198** 132–179
- [38] Ring P, Gambhir Y K and Lalazissis G A 1997 *Comput. Phys. Commun.* **105** 77–97
- [39] Zhao P W, Li Z P, Yao J M and Meng J 2010 *Phys. Rev. C* **82** 054319–14
- [40] Chen Y and Gao Z 2013 *Nucl. Phys. Rev.* **30** 278–283
- [41] Robinson A P, et al. 2008 *Phys. Rev. C* **78** 034308–6
- [42] Chen Y S, Sun Y and Gao Z C 2008 *Phys. Rev. C* **77** 061305(R)–5
- [43] Zhao J, Lu B N, Zhao E G and Zhou S G 2012 *Phys. Rev. C* **86** 057304–4 (*Preprint* 1209.6567)
- [44] Nikšić T, Vretenar D and Ring P 2008 *Phys. Rev. C* **78** 034318–19
- [45] Jolos R V, Malov L A, Shirikova N Y and Sushkov A V 2011 *J. Phys. G: Nucl. Part. Phys.* **38** 115103–